5-19-2014

Ultraviolet laser crystallized ZnO:Al films on sapphire with high Hall mobility for simultaneous enhancement of conductivity and transparency

Qiong Nian
Purdue University, Birck Nanotechnology Center, qnian@purdue.edu

Martin Y. Zhang
Purdue University, Birck Nanotechnology Center

Bradley D. Schwartz
ITC Aerpspace Syst

Gary J. Cheng
Purdue University, Birck Nanotechnology Center, gjcheng@purdue.edu

Ultraviolet laser crystallized ZnO:Al films on sapphire with high Hall mobility for simultaneous enhancement of conductivity and transparency

Qiong Nian, Martin Y. Zhang, Bradley D. Schwartz, and Gary J. Cheng

---

Articles you may be interested in

Room temperature deposition of alumina-doped zinc oxide on flexible substrates by direct pulsed laser recrystallization
Appl. Phys. Lett. **100**, 151902 (2012); 10.1063/1.3702460

Optical and electrical properties of transparent conducting B-doped ZnO thin films prepared by various deposition methodsa)
J. Vac. Sci. Technol. A **29**, 041504 (2011); 10.1116/1.3591348

Modification of transparent conductive ZnO and Ga-doped ZnO films by irradiation with electron cyclotron resonance argon plasma
J. Vac. Sci. Technol. A **29**, 031304 (2011); 10.1116/1.3571603

Effect of fluorine addition on transparent and conducting Al doped ZnO films
J. Appl. Phys. **100**, 063701 (2006); 10.1063/1.2347715

Structural, electrical, and optical properties of transparent conductive oxide ZnO:Al films prepared by dc magnetron reactive sputtering
J. Vac. Sci. Technol. A **19**, 963 (2001); 10.1116/1.1368836

Ultraviolet laser crystallized ZnO:Al films on sapphire with high Hall mobility for simultaneous enhancement of conductivity and transparency

Qiong Nian,[1,2] Martin Y. Zhang,[1,2] Bradley D. Schwartz,[3] and Gary J. Cheng[1,2,4,a]

[1]School of Industrial Engineering, Purdue University, 315N. Grant St, West Lafayette, Indiana 47907, USA
[2]Birck Nanotechnology Center, Purdue University, 1205W State St, West Lafayette, Indiana 47907, USA
[3]Goodrich Corporation, UTC Aerospace Systems, 100 Wooster Heights Road, Danbury, Connecticut 06810, USA
[4]School of Mechanical Engineering, Purdue University, 585 Purdue Mall, West Lafayette, Indiana 47907, USA

One of the most challenging issues in transparent conductive oxides (TCOs) is to improve their conductivity without compromising transparency. High conductivity in TCO films often comes from a high carrier concentration, which is detrimental to transparency due to free carrier absorption. Here we show that UV laser crystallization (UVLC) of aluminum-doped ZnO (AZO) films prepared by pulsed laser deposition on sapphire results in much higher Hall mobility, allowing relaxation of the constraints of the conductivity/transparency trade-off. X-ray diffraction patterns and morphological characterizations show grain growth and crystallinity enhancement during UVLC, resulting in less film internal imperfections. Optoelectronic measurements show that UVLC dramatically improves the electron mobility, while the carrier concentration decreases which in turn simultaneously increases conductivity and transparency. AZO films under optimized UVLC achieve the highest electron mobility of 79 cm^2/V s at a low carrier concentration of $7.9 \times 10^{+19}$ cm^{-3}. This is realized by a laser crystallization induced decrease of both grain boundary density and electron trap density at grain boundaries. The infrared (IR) to mid-IR range transmittance spectrum shows UVLC significantly enhances the AZO film transparency without compromising conductivity. © 2014 AIP Publishing LLC. [http://dx.doi.org/10.1063/1.4879643]

Aluminum-doped ZnO (AZO) is currently under intense investigation and development to replace indium tin oxide (ITO) as a transparent conductive coating. AZO thin films exhibit high electro-optical quality, sufficient material availability, environmental benefits, and low cost to manufacture.[1,2] Meanwhile, the good electro-optical properties and reliability of AZO films lead to wide applications in display windows,[3] thin film solar cells,[4] and optoelectronic devices[5] such as transparent thin film transistors. Various deposition techniques are applied to fabricate AZO films, such as sputtering, chemical vapor deposition, cathodic arc deposition, atomic layer deposition (ALD), and pulsed laser deposition (PLD).[6–14] Some attempts of depositing AZO by low temperature PLD[15–17] for optical devices encounter issues like poor optoelectronic properties. Extended defects like grain boundaries and inter-grain voids play an important role in the electrical properties of AZO films.[18] For instance, these defects may create energy levels in the band gap (traps) that tend to decrease the carrier lifetime so as to decrease the electron mobility.[19] In order to reduce the drawback effect of these defects, post-deposition annealing is utilized to enhance the electrical properties of the AZO film. The enhancement results from alleviating accumulated strain energy and improving crystallinity.[20] However, annealing might cause lower conductivity because of the ionization of oxygen vacancies and the oxidation of aluminum.[21] On the other hand, increasing the optical transparency in the red/infrared (IR) range can be achieved by reducing the carrier

concentration; however, this is usually results in lower conductivity.[22] Thus, high carrier mobility and low carrier concentration are desired for simultaneously achieving high conductivity and extended IR transparency. Some methods are now being developed to relax this conductivity/transparency trade-off by increasing the carrier mobility.[22,23]

In this study, AZO films were deposited on sapphire substrates by room temperature PLD. UV laser crystallization (UVLC) was used to achieve high carrier mobility for improving the conductivity and transmittance, aiming to relax the conductivity/transparency trade-off.

Before PLD, (0001) orientation sapphire substrates were cleaned by acetone, methanol, and DI water in an ultrasonic cleaner for 5 min each, sequentially. A substrate was put into a high vacuum chamber with a base pressure of 4.0×10^{-6} Torr, where ZnO (99.99%) and 2% Al$_2$O$_3$-doped zinc oxide (AZO) targets were ablated by a KrF excimer laser (λ of 248 nm with τ of 25 ns). A 50 nm thick i-ZnO nucleation layer was deposited at laser fluence of 1.5 J/cm^2, repetition rate (RR) of 10 Hz for 20 min, and then 200 nm thick Al-ZnO was deposited on top at 0.5 J/cm^2, 5 Hz for 90 min. O$_2$ pressure was set to be 150 and 1 mTorr for i-ZnO and AZO films, respectively.

As-deposited samples were then transferred into a 10 mTorr vacuum chamber for the UVLC process. The same laser was used with RR of 10 Hz with the beam shaped to a square, top-hat profile (8 × 8mm). The sample was placed on a motorized hotplate stage at 500 K which enabled translations along both X- and Y-axes as shown in Fig. 1(a). Laser fluence applied ranged from 120 to 200 mJ/cm^2 with exposure time 2.5–5 μs, e.g., (25 ns) (100 pulses) = 2.5 μs.

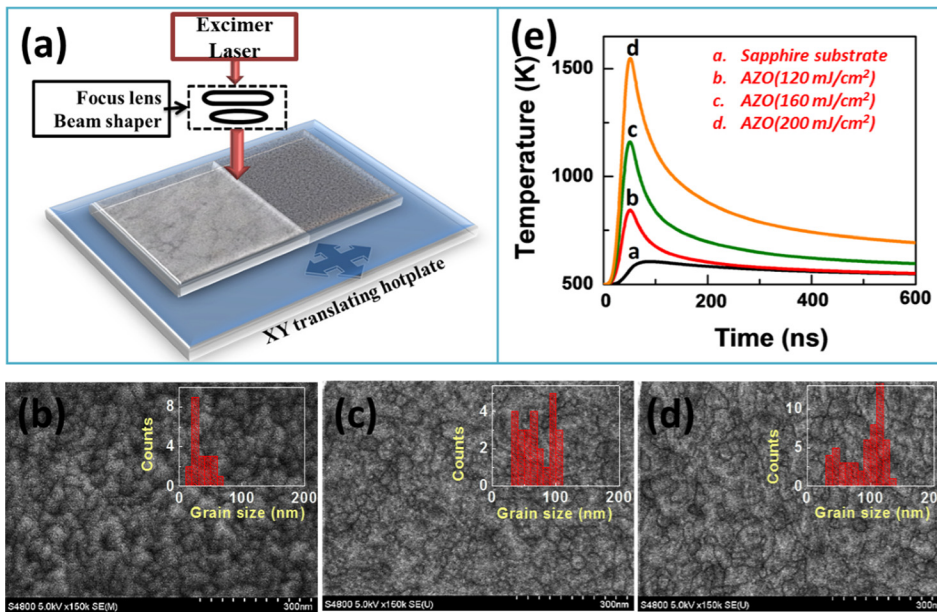a)Author to whom correspondence should be addressed. Electronic mail: gjcheng@purdue.edu. Tel.: 765-494-5436.

FIG. 1. (a) Schematic setup of AZO film UVLC; (b) as-deposited AZO film by PLD; AZO film processed by UVLC (at 500 K): (c) 120 mJ/cm², 5 μs; (d) 160 mJ/cm², 5 μs. Insets in (b)–(d) show grain size distribution. (e) Temperature evolutions of AZO film on sapphire substrate carried out by COMSOL Multiphysics® simulation for a single laser pulse at $\lambda = 248$ nm, $\tau = 25$ ns;

After UVLC, field emission scanning electron microscopy (FE-SEM) and x-ray diffraction patterns (XRD) were used to observe the film morphology and crystallinity. Electrical resistivity, carrier mobility, and carrier concentration were measured by the Hall Effect with the Van der Pauw method. Optical transmittance was measured by UV-visible-IR spectrometers.

Figs. 1(b)–1(d) show the plane-view FE-SEM surface morphology of the AZO film as-deposited by PLD and processed by UVLC (120 mJ/cm² and 160 mJ/cm²) for 5 μs exposure time. It can be seen in Fig. 1(b) that the as-deposited AZO film contains inter-grain defects like voids, gaps, and grain boundaries, exhibiting inhomogeneity and discontinuity.[1,24] Comparing to Fig. 1(c), when UVLC is applied to an AZO film with fluence of 120 mJ/cm² for 5 μs, facetted grains begin to form and impinge with each other, achieving compact and continuous surface, suggesting film quality and crystallinity have been significantly improved.[18,24] Fig. 1(c) subject to UVLC with higher fluence of 160 mJ/cm² for 5 μs exposure shows similar surface morphology such as good film homogeneity and surface flatness. Whereas the facetted grains with boundaries become more apparent, since more thermal energy is delivered for thorough crystallization. Not only grain shapes change but also grain growth is detected. The investigation of grain growth is carried out by observing the grain size distribution as shown in insets of FE-SEM images. It can be observed that higher laser fluence results in better grain growth. In most of the cases, grain size distribution is bi-modal. There is a swift transition of smaller grains into larger grains. On the other hand, at laser fluence higher than the optimum threshold (160 mJ/cm²) window, there is a clear-cut grain growth as compared to the as-deposited film as shown in supporting Fig. 1. Film lack long range crystalline order, as higher laser fluence like 200 mJ/cm² causes ablation of material,[25,26] that is, laser evaporated material would redeposit back on the surface but no crystallization energy is available for them, so that resultant surface would lack crystallinity.

To understand the mechanism of UVLC, COMSOL Multiphysics® was utilized to study the film temperature evolution during a single laser pulse exposure (25 ns),[1] as shown in Fig. 1(e). The initial temperature of the sapphire substrate and AZO film was set at 500 K corresponding to the temperature of the hotplate. Then, an electromagnetic-heat transfer module (EM-HT) was used to simulate the laser exposure and temperature increase. As a result, the temperature of the AZO film increases to 850, 1160, and 1560 K in 60 ns for laser fluence of 120, 160, and 200 mJ/cm², respectively. According to van de Pol et al.,[27] the calibrated melting point of AZO is 1400 K. Thus, the peak temperature of 850–1160 K triggered by the laser fluence of 120–160 mJ/cm² corresponds to 60%–80% of the melting point of the AZO film, which is in the desired range for the crystallization stated by the Thornton structure zone model.[28] As thermal energy continues along longer exposure time, large crystals tend to merge with smaller ones until faceted grains form and impinge with each other. On the other hand, the peak temperature of 1560 K triggered by laser fluence of 200 mJ/cm² is above the melting point of AZO film which causes material ablation.[28]

The improvement in crystallinity of AZO films processed by UVLC was confirmed by XRD patterns, which were collected and analyzed as shown in Figs. 2(a) and 2(b). In Fig. 2(a), the diffraction peaks appearing at 34.5° and 41.7° correspond to the (0002) peak of hexagonal wurtzite structure AZO and the (0006) peak of sapphire, respectively.[29–31] It is well known that (0002) is the dominant orientation in Al doped ZnO films grown by various methods including PLD, sputtering, and CVD.[1,15] No characteristic peaks of metallic Zn, Al, or $ZnAlO_4$ were detected, indicating that the films have highly crystalline structure with a c-axis preferred out-of-plane orientation. After UVLC, the AZO (0002) peak was found to become stronger and stronger associated with laser fluence increase from 0 to 120 mJ/cm² and finally 160 mJ/cm². The stronger peaks attribute to the crystallinity enhancement including a larger grain size and preferable orientation, i.e., low misalignment or tilt along the c-axis. However, a laser fluence of 200 mJ/cm² is too high, which lowers the XRD peak height, implying degraded crystallinity. The well-known Debye-Scherrer Formula was utilized to calculate crystal sizes
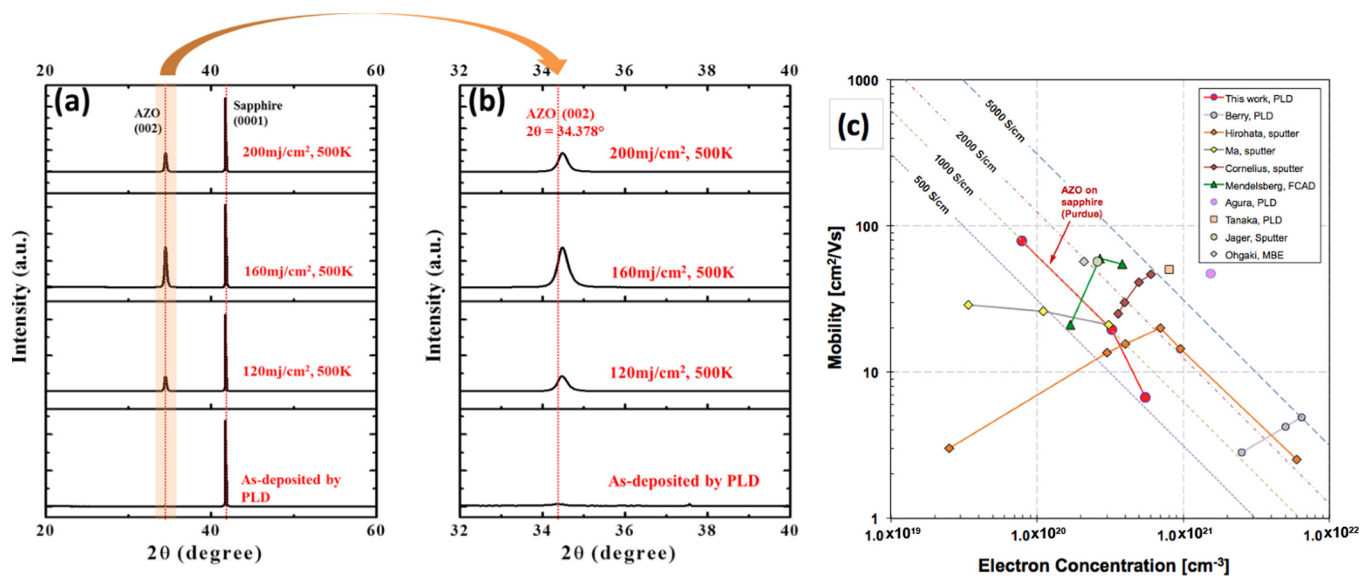
FIG. 2. (a) θ–2θ XRD patterns of AZO films as-deposited by PLD and processed by UVLC at 120 mJ/cm^2, 160 mJ/cm^2, and 200 mJ/cm^2 at 500 K, respectively. The AZO films have a preferred (0002) out-of-plane orientation on the c-plane sapphire substrate. (b) Thermal strain introduced by UVLC. AZO (0002) peak of the crystallized samples show 0.1° high angle shift. (c) Electron mobility vs. electron concentration for AZO films as-deposited by PLD and processed by UVLC, comparing with nine research groups. The red curve shows current work, the other marked points and curves represent high mobility AZO films listed in Table I in supporting materials. The diagonal dashed lines show constant conductivity on a log-log scale.

from the full width at half maximum (FWHM) of the XRD patterns as presented in the right column of Table I. The average crystal size of AZO film increased from 24.9 to 32.4 nm when a laser fluence of 160 mJ/cm^2 and 5 μs exposure is applied. However, a clear-cut crystal size decrease was detected with a fluence of 200 mJ/cm^2, which is not desired.

Furthermore, a 0.1° shift to higher angle of AZO (0002) peak was detected in processed samples as shown in Fig. 2(b) and Table I. This upshift indicates the lattice distortion induced due to strain. The strain most likely originated from the substitution of Al^{3+} for Zn^{2+}.[32,33] For 2% Al doped ZnO film in this work, the Al^{3+} has a smaller radius ($\sim$0.05 nm) than Zn^{2+} ($\sim$0.074 nm), thus leading to a decrease in the lattice constant.[32] The smaller radius of the Al^{3+} brings about higher ion mobility, which drives the Al^{3+} more likely getting across the crystal boundary than Zn^{2+} in UVLC process and resulting in a better crystalline orientation at AZO (0002) peak. Therefore, after UVLC process, the substitution of Al^{3+} to Zn^{2+} is enhanced, causing the crystallinity enhancement and the lattice constant decrease which are shown as AZO (0002) peak strengthening and upshifting in Figs. 2(a) and 2(b).

Due to crystallinity improvement after UVLC, an enhanced electrical conductance was expected. Hall Effect measurements were carried out to investigate the resistivity, mobility, and carrier concentrations each for 3 times, whose mean values are shown in Table II. The resistivity of as-deposited by PLD was measured to be 1.68×10^{-3} Ω-cm,

but decreased to 9.90×10^{-4} Ω-cm after optimized UVLC (160 mJ/cm^2, 5 μs) exposure at 500 K. This reveals UVLC coalescences a few small crystals into larger ones and reorganizes the facetted grains into a compact and homogenous film which decreases the internal defects density that influences polycrystalline AZO film conductance.[1,21,24,34]

To understand the conductance enhanced by UVLC, Hall mobility, and carrier concentration of AZO films as-deposited and processed by optimized fluence (160 mJ/cm^2) with 2.5 μs and 5 μs exposure were analyzed. It is found Hall mobility increases from 6.7 to 19.5 and 79 cm^2/Vs after 2.5 μs and 5 μs exposures. While the carrier concentration decreases from $5.5 \times 10^{+20}$ to $3.2 \times 10^{+20}$ and then $7.9 \times 10^{+19}$ cm^{-3}. The carrier concentration decrease is caused by the non-equilibrium and low-oxygen UVLC process that produces zinc vacancies that then capture excited electrons from the Al dopant and thus lower the carrier density.[35] However, polycrystalline Hall mobility μ_{Hall} depends on intragrain mobility μ_i and grain boundary mobility μ_g, usually dominated by ionized impurity scattering or grain boundary scattering, according to different carrier concentrations.[22,34,36,37] Equation (1) shows the relationship, neglecting neutral impurity scattering, lattice vibration scattering, and intragrain cluster scattering[36]

TABLE I. Peak position, FWHM of XRD AZO (0002) peaks and grain size for as-deposited and processed AZO films.

Sample	Peak position (°)	FWHM (°)	Crystal Size (nm)
As-deposited by PLD	34.378	0.328	24.9
UVLC (120 mJ/cm^2, 500 K)	34.484	0.284	29.1
UVLC (160 mJ/cm^2, 500 K)	34.487	0.255	32.4
UVLC (200 mJ/cm^2, 500 K)	34.476	0.274	30.1

TABLE II. Electrical properties of 200 nm thick n-type AZO films as-deposited and processed by UVLC.

AZO films	Mean resistivity (Ω cm)	Mean Hall mobility (cm^2/Vs)	Mean carrier density (cm^{-3})
As-deposited by PLD	1.68×10^{-3}	6.7	$5.5 \times 10^{+20}$
UVLC (160 mJ/cm^2, 2.5 μs)	9.92×10^{-4}	19.5	$3.2 \times 10^{+20}$
UVLC (160 mJ/cm^2, 5 μs)	9.90×10^{-4}	79.0	$7.9 \times 10^{+19}$
UVLC (200 mJ/cm^2, 5 μs)	1.87×10^{-1}	9.9	$3.4 \times 10^{+20}$

$$\frac{1}{\mu_{hall}} = \frac{1}{\mu_i} + \frac{1}{\mu_g}. \qquad (1)$$

For the relative high carrier concentrations ($>2 \times 10^{20}\,cm^{-3}$), it is generally agreed that mobility is dominated by ion impurity scattering, explaining that the Hall mobility increase from 6.7 to 19.5 cm^2/Vs is mainly due to the carrier concentration decrease from $5.5 \times 10^{+20}$ to $3.2 \times 10^{+20}$ that diminishes ionized impurity scattering.[34,37] However, for the relative low carrier concentration of $7.9 \times 10^{+19}\,cm^{-3}$ after UVLC, the dominant factor is grain boundary scattering, which depends on the grain boundary density and the energy potential barrier (Φ_B) at grain boundaries.[37,38] To describe μ_g, Seto and Baccarani[39,40] extended the Petritz model[41] as presented in the following equation:

$$\mu_g = \mu_0 \exp\left(-\frac{\phi_B}{kT}\right) = \frac{eL}{\sqrt{2\pi m^* kT}} \exp\left(-\frac{e^2 N_t^2}{8kT\varepsilon\varepsilon_0 N_{eff}}\right), \qquad (2)$$

where L is the grain size, N_t is the electron trap density at grain boundaries, N_{eff} is the free electron concentration, m^* is the electron effective mass, $\varepsilon\varepsilon_0$ is the static dielectric constant, and e is the elementary charge. After UVLC, grain size L is enlarged, with an increase factor of $\sim$2 times according to Fig. 1 histograms, which does not explain the significant mobility increase from 6.7 to 79 cm^2/V s. Thus, electron trap density N_t must have been lowered to achieve high mobility. It is well known that extended defects like inter-grain voids, gaps, and grain boundaries might form electron traps at grain boundaries.[18] The UVLC process forms facetted grains that impinge with each other to achieve a compact structure, thereby significantly lowering the internal defect density and decreasing the electron trap density. In addition, prior reports[22,42] also state that UV light exposure is able to desorb oxygen species at grain boundaries, which help decrease electron trap density as well. Both enlarged grain size and decreased electron trap density contribute to Hall mobility enhancement at low carrier concentration.

To demonstrate the performance boost by UVLC, the electrical properties of processed AZO film are compared with prior advancements,[6–14] as shown in Fig. 2(c) (red curve), that is, electron mobility vs. free electron concentration data for AZO thin films deposited by different research groups. It is

well known that as the free carrier concentration increases over $2 \times 10^{+20}\,cm^{-3}$ in polycrystalline AZO films, the traps between grains can be partially or completely filled, reducing the barrier height and width, and thereby increasing Hall mobility. However, for relative low carrier concentration, grain boundary scattering modification would play dominant role in Hall mobility enhancement. When a carrier density of $7.9 \times 10^{+19}\,cm^{-3}$ is fixed, the UVLC processed AZO film obtains higher carrier mobility than previous reports, indicating a diminishing grain boundary barrier or decreasing grain boundary density. Additionally, grain boundary density also could be affected by film thickness which would further influence the carrier mobility.[22] Considering the 200 nm thick film in our work is thinner than prior advancements, UVLC has a potential to achieve even higher Hall mobility.

It has been proven that high Hall mobility is necessary for relaxing the conductivity/transparency trade-off, that is, increasing the transparency in the red/IR range can be readily achieved by reducing the impurity doping level without the expense of conductivity.[22] High Hall mobility satisfies electrical conductance requirements even at lower impurity doping levels. The transmittance spectra of UVLC samples on sapphire were collected to compare with as-deposited ones as shown in Fig. 3. As observed, the transmittance of an as-deposited film decreases in the red to near IR (NIR) region (750–1500 nm) because of increasing reflectance and free carrier absorption.[43] While, UVLC dramatically enhances the red/IR transmittance in the wavelength range of 750–1500 nm for processed samples as shown in Fig. 3(a). The enhanced red/IR transmittance attributes to decreasing reflectance and free carrier absorption, resulting from improved film flatness and diminished carrier concentration.[44] UVLC with all three fluences shows the capability to boost red/IR (700–1500 nm) transmittance. The electrically optimal condition with fluence of 160 mJ/cm^2 achieves the strongest enhancement in IR transmittance: over 21% average transmittance increase in the wavelength range 900–1500 nm, subject to a significantly decreased carrier concentration. In order to further demonstrate the feasibility of an optimally processed sample as an infrared transparent conductor for windows and optoelectronic devices, transmittance measurements from 350–8000 nm were conducted as shown in Fig. 3(b). It is found that in the NIR to
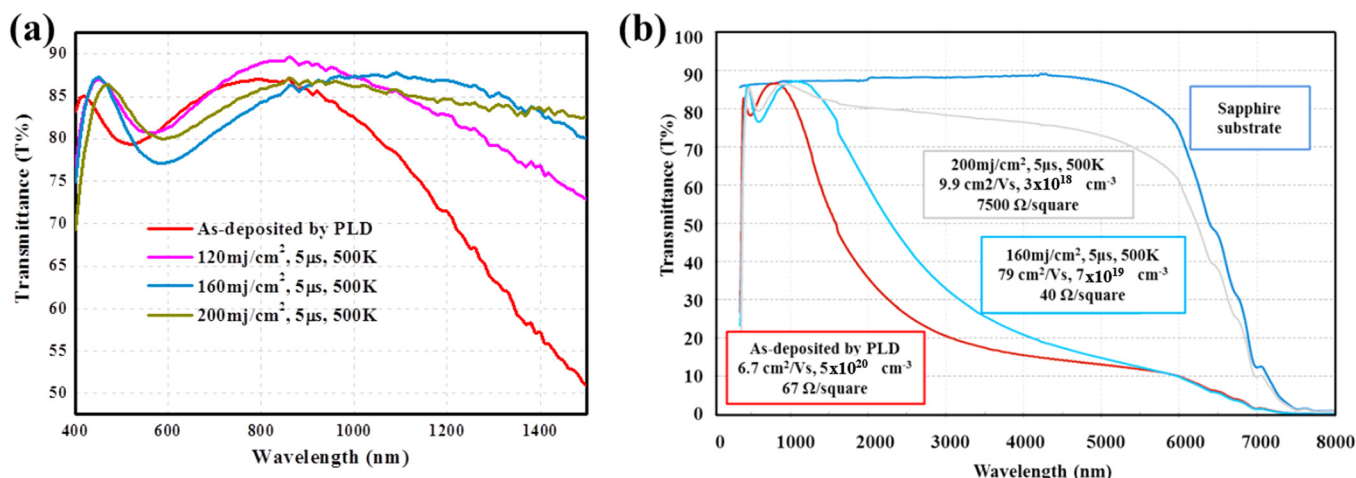

FIG. 3. (a) Effect of laser crystallization conditions on UV to near IR transmittance spectra of AZO films; (b) UV to mid wave IR transmittance spectra of uncoated sapphire substrate and AZO films deposited by room temperature PLD ($R_S = \sim$67 Ω/sq) and processed by UVLC ($R_S = \sim$40 Ω/sq and $\sim$7500 Ω/sq).

mid wave IR (MWIR) region (900–5000 nm), the average transmittance increase of 36% is achieved under 160 mJ/cm^2, implying a decreased internal defects level and reduced free carriers.[44] This transparency improvements are associated with decreased carrier concentration, but increased Hall mobility, and decreased sheet resistance (from 67 Ω/sq to 40 Ω/sq), without any expense of conductance, which relaxes the conductivity/transparency trade-off.[22] Considering the light absorption of sapphire, the sole AZO film of current series of samples can achieve even higher transparency, which is comparable or higher, as compared with previous literatures.[43–47]

However, too high fluence like 200 mJ/cm^2 reduced the film conductance back to a low level (Fig. 3(b)), demonstrating that extra thermal energy beyond optimal fluence degrades the film quality, though the mid-IR transmittance is dramatically increased over 60% to 6000 nm wavelength (grey curve in Fig. 3(b)) due to an intensively decreased carrier concentration.

Optical interference effects in these thin films change the transmittance at shorter wavelengths. As shown in Fig. 3(a), the transmittance minimum shifted from 78.2% at 490 nm to 76.5% at 590 nm because the film became denser with fewer voids after laser processing. The shift to a longer wavelength and the greater difference between the peak and valley transmittance in the processed film indicate a higher index of refraction and lower free carrier absorption than the as-deposited film. The peak transmittance is equal to that of the sapphire substrate indicating very low absorption loss for $450 < \lambda < 1100$ nm in the UVLC samples.

In a summary, UVLC was applied to transparent and conductive AZO films prepared by room temperature PLD. This technique is able to solve the problem of compromised transparency while increasing conductivity in transparent conductive oxide (TCO) layers. After UVLC, high quality AZO films were produced with high Hall mobility of 79 cm^2/Vs, and low carrier concentration of $7.9 \times 10^{+19}$ cm^{-3}, resulting in relaxation of constraint in conductivity/transparency trade-off. The near to mid IR range transmittance from 900–5000 nm of this UVLC processed AZO film ($R_S = 40$ Ω/sq) was dramatically enhanced, around 36% higher than as-deposited AZO ($R_S = 67$ Ω/sq).

[1]M. Y. Zhang and G. J. Cheng, Appl. Phys. Lett. **99**(5), 051904 (2011).
[2]T. Minami, S. Suzuki, and T. Miyata, Thin Solid Films **398–399**(0), 53 (2001).
[3]S. Takata, T. Minami, and H. Nanto, Thin Solid Films **135**(2), 183 (1986).
[4]W.-J. Jeong and G.-C. Park, Sol. Energy Mater. Sol. Cells **65**(1–4), 37 (2001).
[5]H. Kim, C. M. Gilmore, J. S. Horwitz, A. Piqué, H. Murata, G. P. Kushto, R. Schlaf, Z. H. Kafafi, and D. B. Chrisey, Appl. Phys. Lett. **76**(3), 259 (2000).
[6]T. Ohgaki, Y. Kawamura, T. Kuroda, N. Ohashi, Y. Adachi, T. Tsurumi, F. Minami, and H. Haneda, Key Eng. Mater. **248**, 91 (2003).
[7]K. Hirohata, N. Oka, Y. Sato, I. Yamamoto, and Y. Shigesato, in "Layer-by-layer Self-assembly of Unilamellar Nanosheet Crystallites of Ruthenium Oxides" in Transparent Conductors and Semiconductors for Optoelectronics, edited by J. D. Perkins, T. O. Mason, J. F. Wager, and Y. Shigesato (Mater. Res. Soc. Symp. Proc. Vol. 1109E, Warrendale, PA, 2009), B03-21.
[8]J. J. Berry, D. S. Ginley, and P. E. Burrows, Appl. Phys. Lett. **92**(19), 193304 (2008).
[9]G. Ma, D. Li, H. Ma, J. Shen, C. Wu, J. Ge, S. Hu, and N. Dai, Appl. Phys. Lett. **93**(21), 211101 (2008).
[10]S. Jäger, B. Szyszka, J. Szczyrbowski, and G. Bräuer, Surf. Coat. Technol. **98**(1–3), 1304 (1998).
[11]S. Cornelius, M. Vinnichenko, N. Shevchenko, A. Rogozin, A. Kolitsch, and W. Möller, Appl. Phys. Lett. **94**(4), 042103 (2009).
[12]H. Tanaka, K. Ihara, T. Miyata, H. Sato, and T. Minami, J. Vac. Sci. Technol., A **22**(4), 1757 (2004).
[13]H. Agura, A. Suzuki, T. Matsushita, T. Aoki, and M. Okuda, Thin Solid Films **445**(2), 263 (2003).
[14]R. J. Mendelsberg, S. H. N. Lim, Y. K. Zhu, J. Wallig, D. J. Milliron, and A. Anders, J. Phys. D: Appl. Phys. **44**(23), 232003 (2011).
[15]C. Guillén and J. Herrero, Vacuum **84**(7), 924 (2010).
[16]K. Matsubara, P. Fons, K. Iwata, A. Yamada, and S. Niki, Thin Solid Films **422**(1–2), 176 (2002).
[17]A. V. Singh, R. M. Mehra, N. Buthrath, A. Wakahara, and A. Yoshida, J. Appl. Phys. **90**(11), 5661 (2001).
[18]Z. Zhang, C. Bao, S. Ma, and S. Hou, Appl. Surf. Sci. **257**(17), 7893 (2011).
[19]D. C. Look, B. Coşkun, B. Claflin, and G. C. Farlow, Phys. B: Condens. Matter **340–342**(0), 32 (2003).
[20]R. J. Lad, P. D. Funkenbusch, and C. R. Aita, J. Vac. Sci. Technol. **17**(4), 808 (1980).
[21]M. A. Al-Maghrabi, M. F. Al-Kuhaili, S. M. A. Durrani, and I. A. Bakhtiari, J. Vac. Sci. Technol., A **27**(2), 276 (2009).
[22]L. Ding, S. Nicolay, J. Steinhauser, U. Kroll, and C. Ballif, Adv. Funct. Mater. **23**(41), 5177 (2013).
[23]L. Ding, M. Boccard, G. Bugnon, M. Benkhaira, S. Nicolay, M. Despeisse, F. Meillaud, and C. Ballif, Sol. Energy Mater. Sol. Cells **98**(0), 331 (2012).
[24]M. Y. Zhang, Q. Nian, and G. J. Cheng, Appl. Phys. Lett. **100**(15), 151902 (2012).
[25]Y. Geng, Z. Y. Xie, S. S. Xu, Q. Q. Sun, S. J. Ding, H. L. Lu, and D. W. Zhang, ECS J. Solid State Sci. Technol. **1**(3), N45 (2012).
[26]M. Y. Zhang, Q. Nian, Y. Shin, and G. J. Cheng, J. Appl. Phys. **113**(19), 193506 (2013).
[27]F. C. M. van de Pol, F. R. Blom, and Th. J. A. Popma, Thin Solid Films **204**(2), 349 (1991).
[28]J. A. Thornton, J. Vac. Sci. Technol. **11**(4), 666 (1974).
[29]O. Bamiduro, H. Mustafa, R. Mundle, R. B. Konda, and A. K. Pradhan, Appl. Phys. Lett. **90**(25), 252108 (2007).
[30]T. Sahoo, J.-W. Ju, V. Kannan, J. S. Kim, Y.-T. Yu, M.-S. Han, Y.-S. Park, and I.-H. Lee, Mater. Res. Bull. **43**(3), 502 (2008).
[31]Y. Hwang, H. Kim, and Y. Um, Curr. Appl. Phys. **12**, S76 (2012).
[32]J. Zhang and W. Que, Sol. Energy Mater. Sol. Cells **94**(12), 2181 (2010).
[33]A. Aprilia, P. Wulandari, V. Suendo, Herman, R. Hidayat, A. Fujii, and M. Ozaki, Sol. Energy Mater. Sol. Cells **111**, 181 (2013).
[34]K. Ellmer, in Transparent Conductive Zinc Oxide, edited by K. Ellmer, A. Klein, and B. Rech (Springer Berlin Heidelberg, 2008), Vol. 104, p. 35.
[35]Z. Zhan, J. Zhang, Q. Zheng, D. Pan, J. Huang, F. Huang, and Z. Lin, Cryst. Growth Des. **11**(1), 21 (2011).
[36]J. G. Lu, Z. Z. Ye, Y. J. Zeng, L. P. Zhu, L. Wang, J. Yuan, B. H. Zhao, and Q. L. Liang, J. Appl. Phys. **100**(7), 073714 (2006).
[37]A. E. Delahoy and S. Guo, Handbook of Photovoltaic Science and Engineering (John Wiley & Sons, Ltd, 2011), p. 716.
[38]T. Minami, MRS Bull. **25**(08), 38 (2000).
[39]J. Y. W. Seto, J. Appl. Phys. **46**(12), 5247 (1975).
[40]G. Baccarani, B. Riccò, and G. Spadini, J. Appl. Phys. **49**(11), 5565 (1978).
[41]R. L. Petritz, Phys. Rev. **104**(6), 1508 (1956).
[42]H. Hagendorfer, K. Lienau, S. Nishiwaki, C. M. Fella, L. Kranz, A. R. Uhl, D. Jaeger, L. Luo, C. Gretener, S. Buecheler, Y. E. Romanyuk, and A. N. Tiwari, Adv. Mater. **26**(4), 632 (2014).
[43]Z. Ben Ayadi, L. El Mir, K. Djessas, and S. Alaya, Mater. Sci. Eng., C **28**(5–6), 613 (2008).
[44]D. Dimova-Malinovska, N. Tzenov, M. Tzolov, and L. Vassilev, Mater. Sci. Eng., B **52**(1), 59 (1998).
[45]T. Ootsuka, Z. Liu, M. Osamura, Y. Fukuzawa, R. Kuroda, Y. Suzuki, N. Otogawa, T. Mise, S. Wang, Y. Hoshino, Y. Nakayama, H. Tanoue, and Y. Makita, Thin Solid Films **476**(1), 30 (2005).
[46]Y. Okuhara, T. Kato, H. Matsubara, N. Isu, and M. Takata, Thin Solid Films **519**(7), 2280 (2011).
[47]T. Dhakal, A. S. Nandur, R. Christian, P. Vasekar, S. Desu, C. Westgate, D. I. Koukis, D. J. Arenas, and D. B. Tanner, Sol. Energy **86**(5), 1306 (2012).